Oxidation of Nitinol

Zhu, Fino, Pelton

Proceedings of SMST-2003
Monterey, CA
(eds.) T.W. Duerig, A. Pelton

2003

OXIDATION OF NITINOL

Lucy Zhu,[1] Jennifer M. Fino,[2] and Alan R. Pelton[1]

[1]Nitinol Devices & Components, 47533 Westinghouse Drive, Fremont, CA 94539
[2]California Polytechnic State University, San Luis Obispo, CA 93407

ABSTRACT
This study explores the kinetics and phase transformations of oxide formation in NiTi. Electropolished Ni-50.8 at% Ti wires were heat treated between 400 and 1000°C for 3 to 300 minutes in air. Surface analytical techniques were used to characterize the thickness, composition and phase distribution of the oxide surface layers. It was observed that the oxide growth is parabolic with a resultant activation energy of 50 kcal/mol, which is comparable to the oxidation of pure Ni and Ti. The results of this study suggests that oxidation occurs as follows:

$$NiTi + O_2 \rightarrow Ni_3Ti + TiO_2 \rightarrow Ni_4Ti + TiO_2 \rightarrow Ni + TiO_2$$

The presence, amount, and distribution of these phases depend on both time and temperature. The composition of the oxides and how it influences biocompatibility are discussed.

KEYWORDS
Nitinol, oxidation, heat treatment, kinetics, phase transformation, corrosion

INTRODUCTION
A number of authors have discussed the unique material properties and biocompatibility that NiTi offers [1-5]. The nearly nickel-free TiO_2 layer of electropolished NiTi has been proven to be an excellent source of corrosion protection; however, the release of nickel ions during the degradation of NiTi is a significant concern when considering its use as an implant material [5-6]. At elevated temperatures in air, titanium reacts with oxygen to form a TiO_2 layer, and the structure of this oxide is important in understanding the biocompatibility of the material. Several authors [7-11] have studied the effects of surface treatments on the surface composition of NiTi, but the mechanisms of high temperature oxidation and the effects on corrosion are not entirely understood. This study investigates the phenomena of oxide formation by means of various surface analytical techniques, and includes the exploration of oxidation kinetics as well as an assessment of the effects on biocompatibility.

EXPERIMENTAL METHODS AND TECHNIQUES
Three mm diameter Ni-50.8 at% Ti wire was annealed at 1000°C for 30 minutes, centerless ground to remove the resultant oxide scale, and electropolished. The wire was subsequently oxidized in an air furnace at 400 to 1000°C in 100°C increments for 3, 10, 30, 100, and 300 minutes. Auger Electron Spectroscopy (AES), Focused Ion Beam (FIB), JEOL JSM-5600 Scanning Electron Microscope (SEM), and Oxford Instruments Model 6587 Energy Dispersive X-Ray Spectroscopy (EDXS) were used to characterize the thickness and composition of the oxide layer(s). AES was used for oxide layers up to 0.1μm; FIB between 0.1-1 μm; and SEM was used for ≥ 1 μm layers. Cross-sections of the wires were prepared using standard metallographic techniques. Two sections of wire from each heat treatment condition were mounted in bakelite, polished to a mirror-like finish with 60 grit to 1200 grit SiC paper, and cleaned in ultrasonicated denatured alcohol. Samples were not etched in order to ensure that all phases were retained for analysis.

Specimens were observed by SEM in both secondary electron imaging (SEI) and backscattered electron imaging (BEI) modes; the BEI mode was especially useful to differentiate Ni-rich (light) and Ti-rich (dark) phases. Layer thickness measurements from AES were based on estimates from the FWHM depth profiles, whereas thicknesses from FIB and SEM were based on averages of measurements from several samples.

RESULTS AND DISCUSSION

OXIDATION GROWTH AND COMPOSITION

No visible oxide was observed by SEM for samples at lower temperatures (≤600˚C) and at 700°C for shorter times (≤30 minutes). These samples were analyzed with AES and/or FIB to determine the oxide thickness and composition. Figure 1 shows the AES depth profile of the electropolished and 400˚C/3 min samples, with a TiO_2 thickness of 110 Å and 200 Å, respectively. After 30 minutes at 400°C, AES revealed a nickel-rich region beneath the outer TiO_2 layer (Figure 2). The remaining samples analyzed with AES showed a more pronounced nickel-rich region below the TiO_2 layer. Table 1 summarizes the oxide thicknesses as a function of temperature and time; the analytical technique used is also indicated.

Table 1: Oxide thickness as a function of temperature and time with analytical technique.

	Temperature (°C)						
	400	500	600	700	800	900	1000
Time (min.)	Oxide Thickness (μm)						
0	0.0110 **A**	0.0110 **A**	0.0110 **A**	0.0110 **A**	0.0110 **A**	0.0110 **A**	0.0110 **A**
3	0.0200 **A**	0.0188 **A**	0.0338 **A**	0.180 **A**	2.737 **S**	6.052 **S**	11.23 **S**
10	0.0338 **A**	0.0244 **A**	0.0808 **F**	0.550 **F**	5.775 **S**	11.40 **S**	21.90 **S**
30	0.0282 **A**	0.0676 **F**	0.534 **F**	0.738 **S**	13.70 **S**	14.70 **S**	54.80 **S**
100	0.0470 **F**	0.0708 **F**	1.356 **F**	2.230 **S**	15.33 **S**	23.50 **S**	157 **S**
300	0.0670 **F**	0.0714 **S**	2.650 **S**	6.780 **S**	20.92 **S**	43.80 **S**	278 **S**

*Primary Analytical Technique: **A** = AES, **F** = FIB, and **S** = SEM

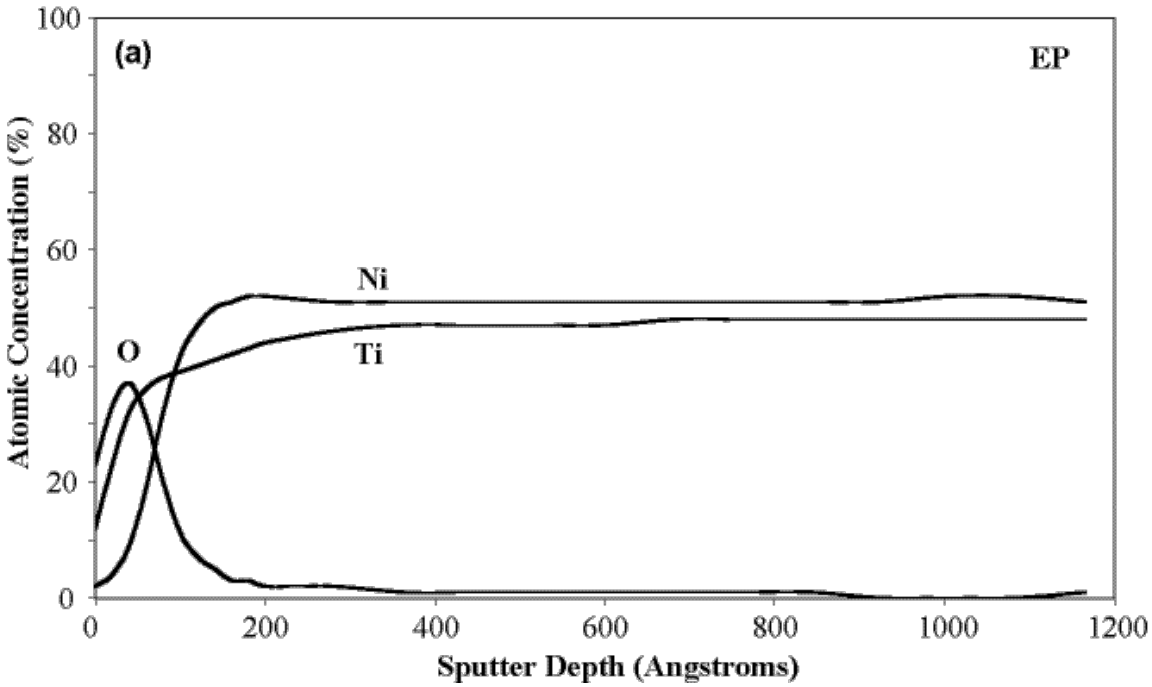

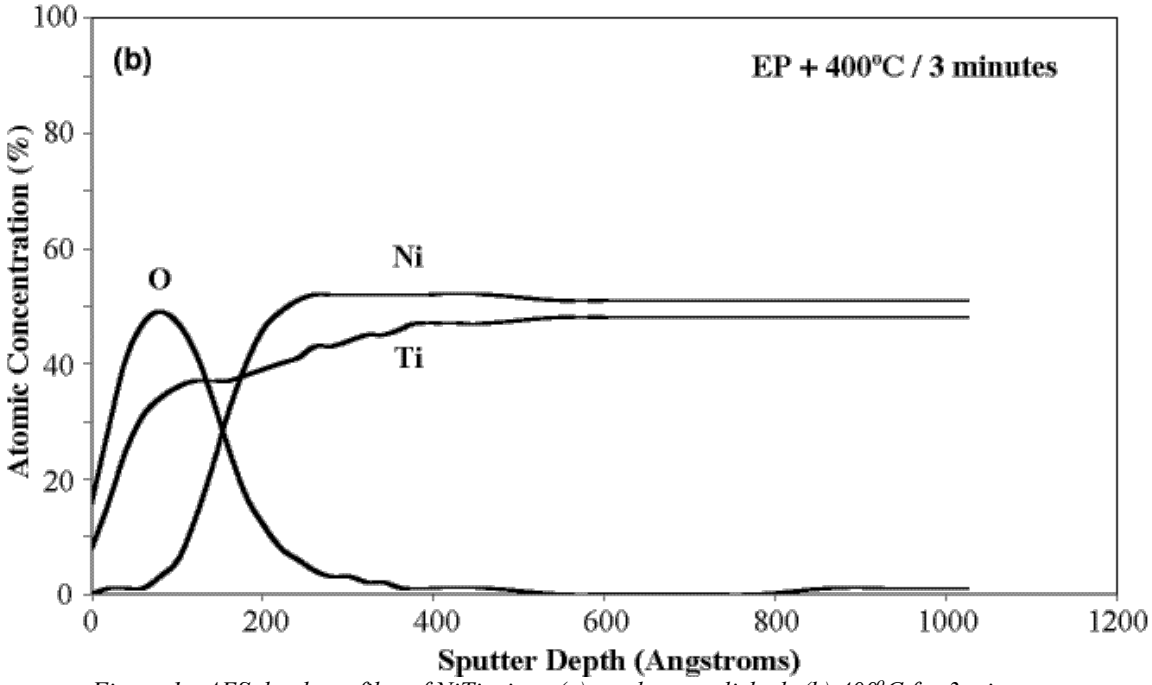

Figure 1: AES depth profiles of NiTi wire: (a) as electropolished; (b) 400°C for 3 minutes.

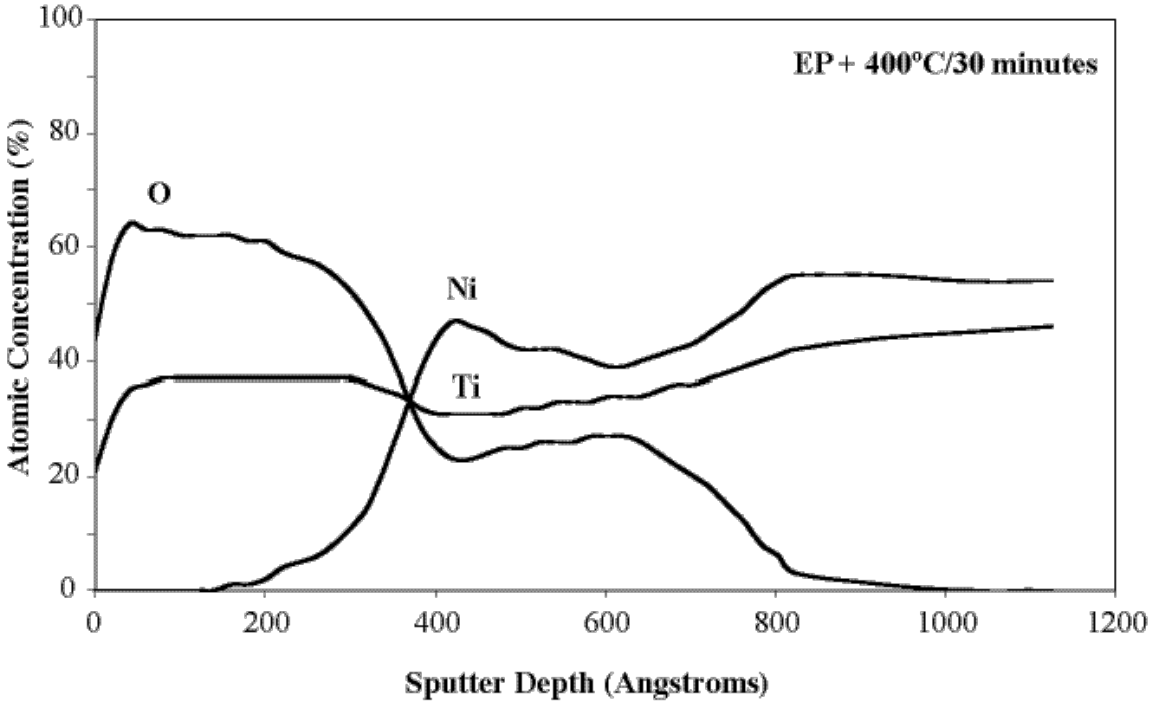

Figure 2: AES depth profile of 400˚C/30 minute NiTi wire. Note the presence of a Ni-rich region below the TiO_2 surface layer.

FIB [12] was used to analyze intermediate oxide thicknesses, as well as to overlap other analysis techniques. Figure 3 shows two light gray superficial platinum layers (marked) that are used as a protective coating during sample preparation. Beneath those layers, a darker TiO_2 (or other Ti suboxide layers) with a lighter nickel-rich sublayer is detected. Chuprina [7] also discovered a "white layer" beneath the surface scale by optical metallography, which he determined to be Ni_3Ti. Voids in the surface layers are also seen in Figure 3. The formation of voids and/or pores may be due to stress generation in the oxide during growth or by the Kirkendall effect whereby vacancies are created when the Ti atoms diffuse away from the NiTi

matrix to react with O_2 [7,13-15]. Chu *et al.* [14] suggest that the formation of large voids may be due to the difference in the vertical and lateral oxide growth rates, as well as the collection of vacancies.

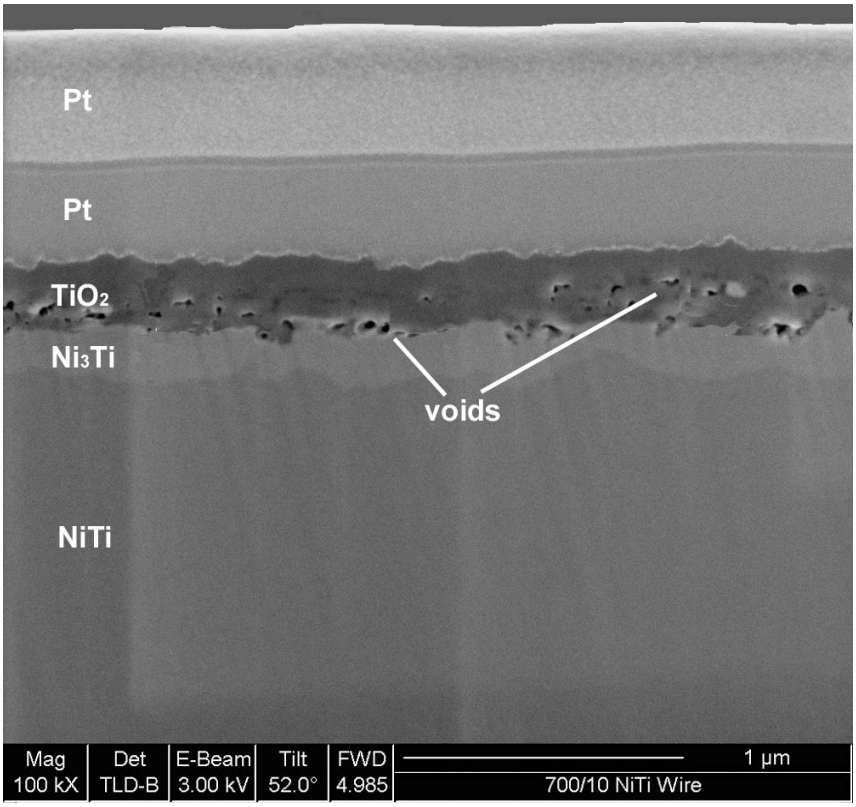

Figure 3: FIB image of 700°C/10 minute NiTi at 100,000X. Note the bright Ni_3Ti layer and (dark) voids.

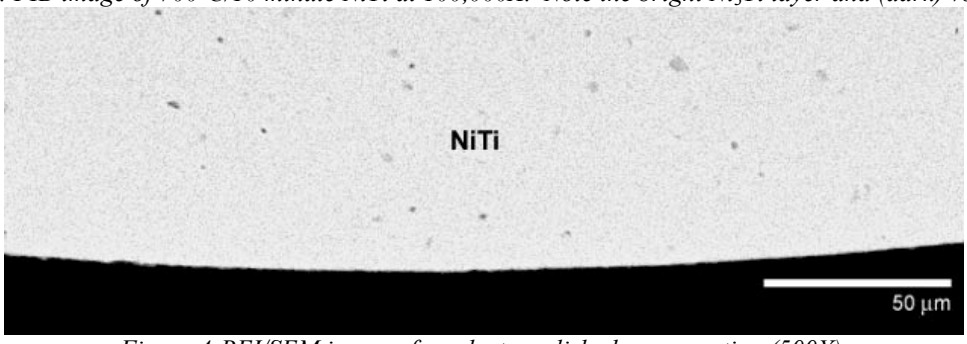

Figure 4:BEI/SEM image of as-electropolished cross-section (500X).

Figure 4 shows the cross-section of the as-electropolished wire, as compared to Figure 5, which illustrates the progressive growth of the oxide with increasing time at 900˚C. The bright interfacial region between the base NiTi and the surface TiO_2 observed for the oxidized samples was analyzed by EDXS to be 75at% Ni and 25at% Ti, consistent with Ni_3Ti (white sublayer); EDXS also confirms the presence of TiO_2 (dark gray). Small Ni_3Ti finger-like projections emerge from the nickel-rich layer and appear to form islands in the oxide. A comprehensive EDXS analysis indicates that the Ni content of the phases increases with increasing distance from the NiTi interface. The Ni_3Ti interfacial layer transforms to Ni_4Ti (80 at% Ni), whereas the islands become nearly pure Ni (approximately 92 at% Ni). This composition transition indicates that with increasing time at temperature, the Ni_3Ti sublayer becomes Ti-depleted as the Ti reacts with the O_2, leaving behind nearly pure Ni. The light gray areas embedded in the TiO_2 observed in Figure 5e may be NiO and TiO_2, which can react to form the double-oxide $NiTiO_3$ [16]. Other authors [7-9,13-14] obtained similar results, but there are discrepancies in the actual composition of these phases. X-ray diffraction analysis in Chuprina *et al.* showed the co-existence of Ni_3Ti, Ni, NiO, Ni(Ti), and TiO_2 at high

temperatures (>600˚C) [7]. Metallic Ni, oxidized Ni, or Ti atoms in solid solution with Ni (Ni(Ti)) have also been reported [9, 13-14].

After 3 minutes at 1000°C, the nickel-rich and titanium oxide regions can be easily observed by BEI/SEM (see Figure 6a). The nickel-rich precipitates and TiO_2 form a lamellar structure of alternating Ni-rich phases and TiO_2. After 30 minutes at 1000°C, this structure becomes more apparent (see Figure 6b), and after 300 minutes at 1000°C, the oxide has become extremely thick (approximately 300 μm), with most of the Ni from Ni_3Ti dispersing into the TiO_2 layer (see Figure 6c). As Ni diffuses to the surface, it becomes increasingly pure (approximately 98at% Ni), with most of the Ti reacting with O_2 to form TiO_2.

It appears that the TiO_2 layer acts as a diffusion barrier to prevent Ni from oxidizing as expected from pure metal thermodynamics [17]. This is also consistent with the thermodynamic calculations from Firstov *et al*. [13], which indicate that reactions at the NiTi/air interface consist of $NiTiO_3$, TiO_2, and metallic Ni, whereas NiO would not be formed due to insufficient oxygen partial pressures.

OXIDATION KINETICS

Figure 7 illustrates the effect of time and temperature on oxide thickness from the present experimental study. Note that there is an initial high growth rate followed by slower growth kinetics at all temperatures. These data also demonstrate the expected trend of higher oxidation rates at higher temperatures. These observations are consistent with a model of oxygen absorption on the NiTi surface that reacts with outward diffusing Ti to form TiO_2. Chu *et al.* [14] and Keng *et al.* [16] discussed the relative direction of atomic diffusion and phase formation. During the early stages of oxidation, the growth of the TiO_2 layer is the only contributor to thickness and therefore oxide formation is relatively rapid. However, the preferential oxidation of Ti creates a Ti-depleted (Ni-rich) zone at the $NiTi/TiO_2$ interface as illustrated in Figures 3-6 above. The formation of the Ni-rich layer increases the effective diffusion distance with a associated decrease in overall oxidation kinetics. Continued oxide growth therefore involves simultaneous nucleation and growth of titanium oxides and Ni-rich phases. Ultimately, these processes lead to the formation of a protective oxide scale, which prevents further oxidation of the base material.

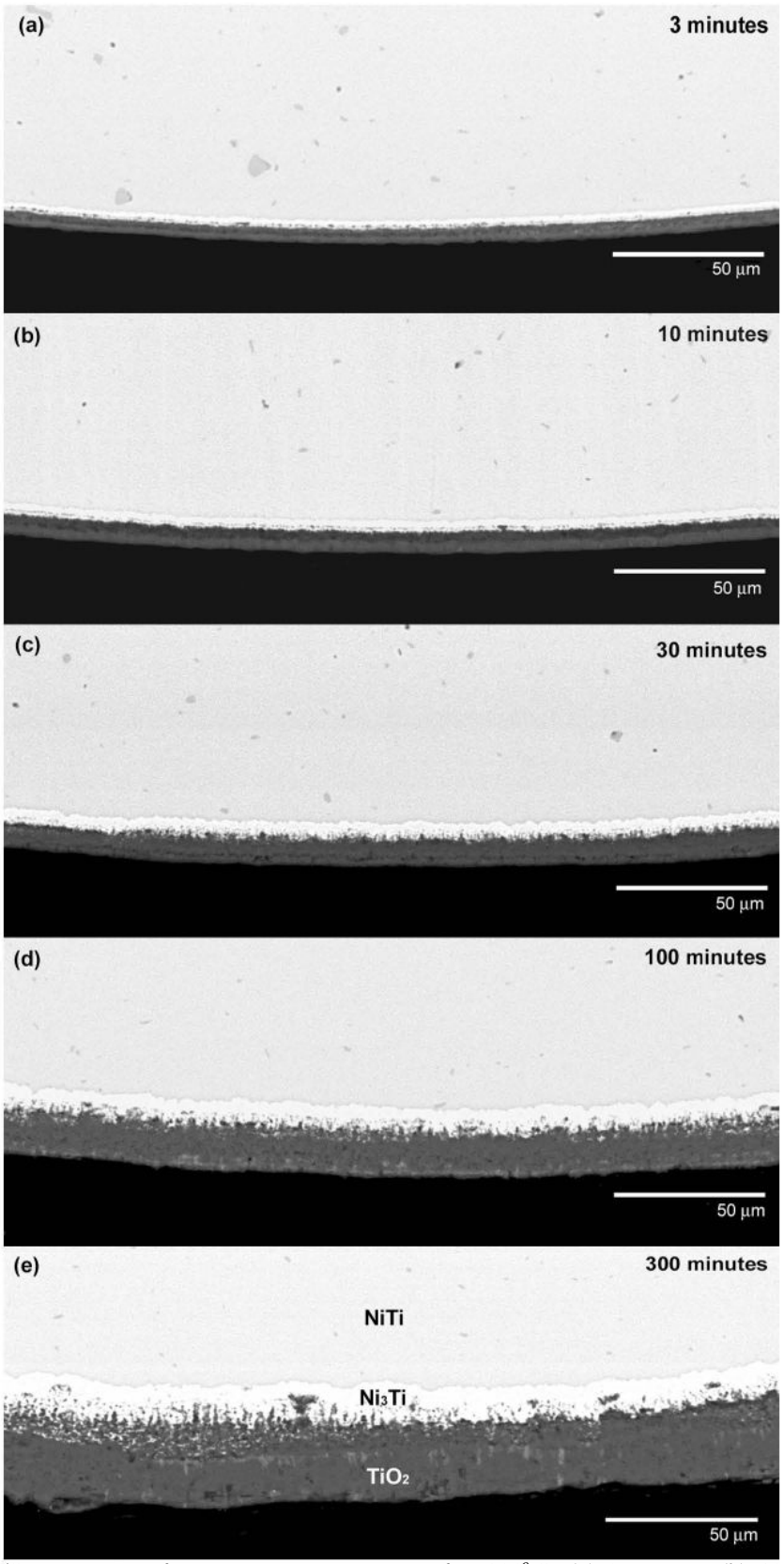

Figure 5: BEI/SEM images of NiTi wire cross-section after 900°C: (a) 3 minutes (b) 10 minutes (c)30 minutes (d) 100 minutes (e) 300 minutes. (500X)

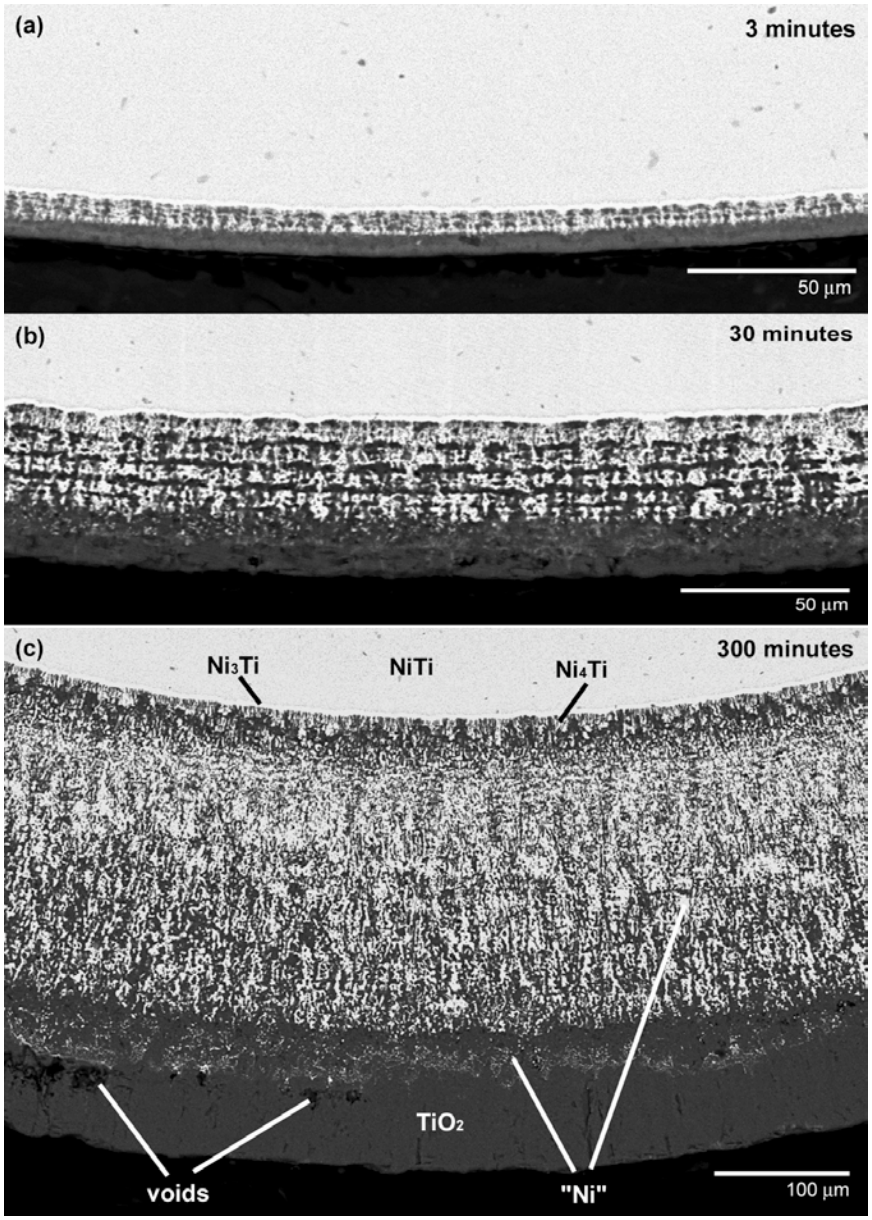

Figure 6: BEI/ SEM image of NiTi wire cross-section after electropolishing and a heat-treatment at 1000°C: (a) 3 minutes (500X), (b) 30 minutes (500X), (c) 300 minutes (200X).

Several authors observed parabolic oxidation rates in NiTi alloys [13-14,16,18]. The governing equation can be written as:

$$thk^2 = k_p t \tag{1}$$

which indicates that square of the oxide thickness (***thk²***) is proportional to time, ***t***, through k_p, the parabolic oxidation rate. Oxidation rates were determined from the data shown in Figure 7. For illustrative purposes, these data were plotted on a log scale. These data can also be modeled with an Arrhenius equation, shown as equation 2, which governs the reaction rates:

$$k_p = k_o \exp\left(-Q/RT\right) \tag{2}$$

where k_o is the rate constant, ***Q*** is the activation energy, ***R*** is the gas law constant, and ***T*** is the absolute temperature. Figure 8 plots the rate constant as a function of 1/T for the seven data sets. An activation

energy of 50 kcal/mol was determined from the slope of the curve. This oxidation activation energy is the same order of magnitude as the activation energy to form NiO from pure Ni (45 kcal) and TiO_2 from pure Ti (26 kcal) [19]; these curves are also shown in Figure 8 for comparison. Chu *et al.* [14] obtained an activation energy of 54 kcal/mol (700-1000°C), which agrees well with the present findings. Chuprina *et al.* [7] found a range of activation energies for various heat treatment temperatures with a transition from low-temperature (600-700°C) oxidation (43 kcal/mol) to high-temperature (700-1000°C) oxidation (72 kcal/mol), which are also consistent with the present data.

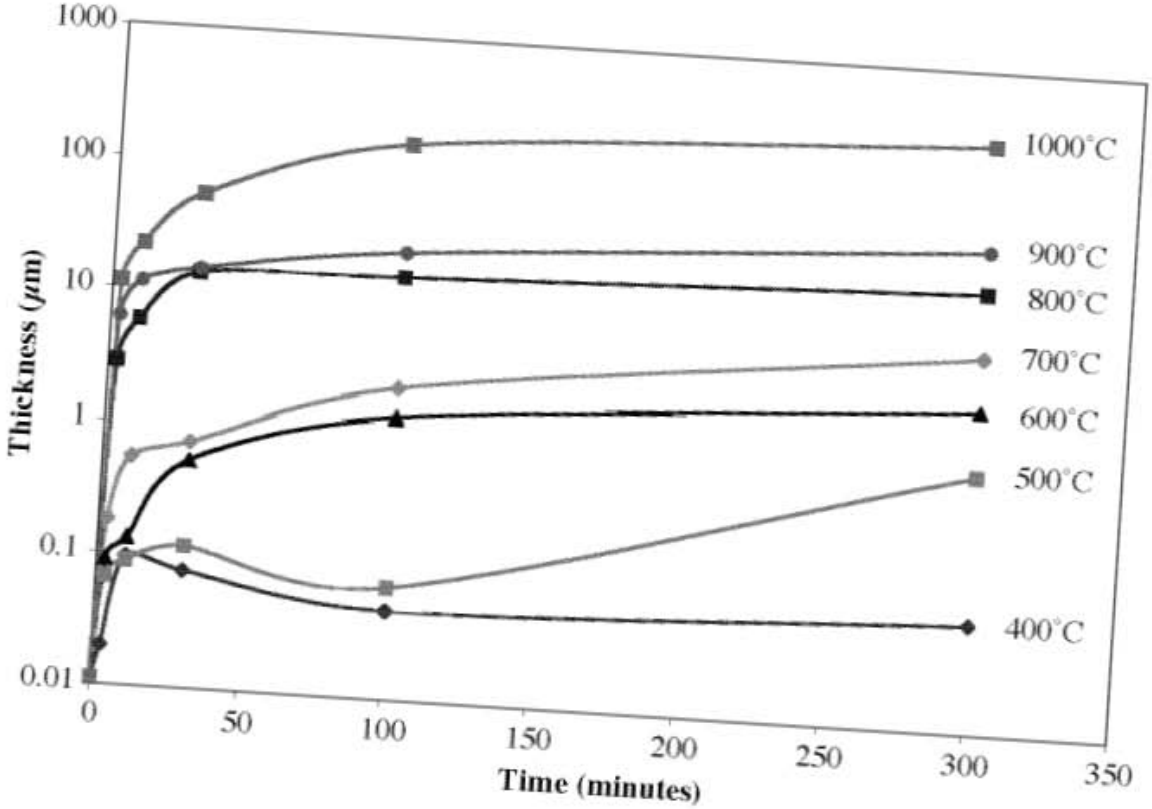

Figure 7: The effect of time on oxide thickness is consistent with parabolic oxide growth.

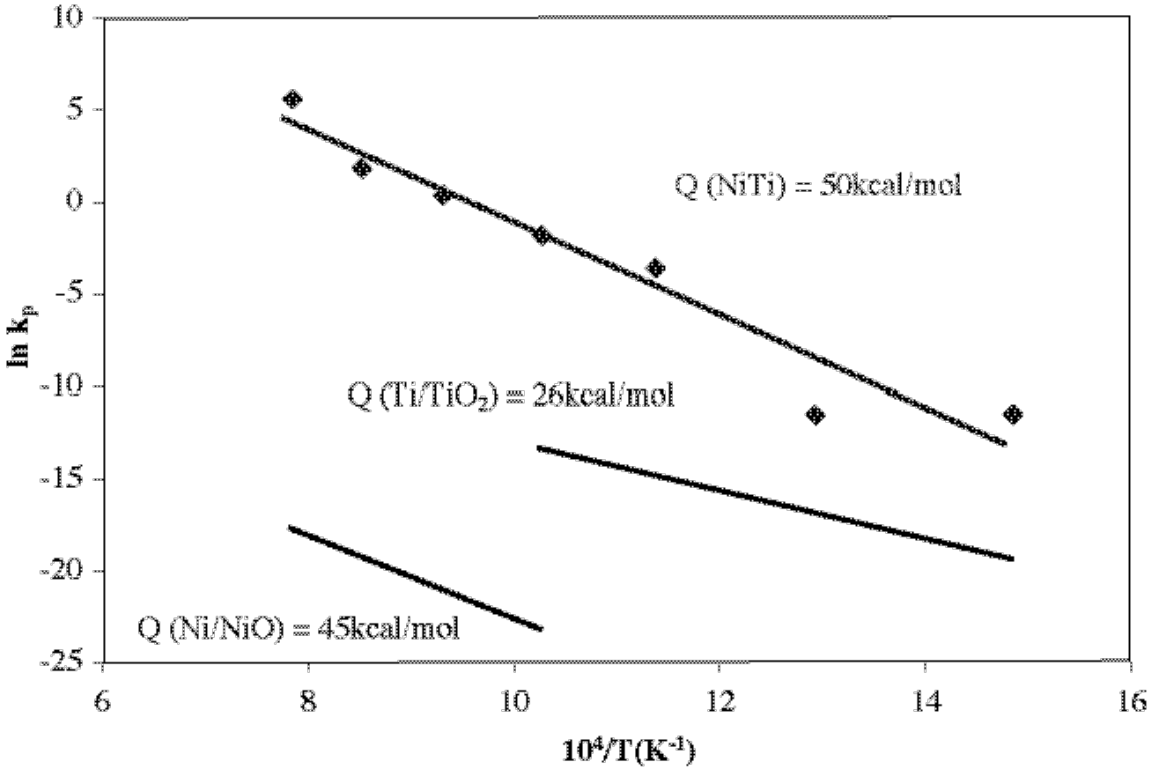

Figure 8: Arrhenius comparison of the oxidation rates for NiTi and Ti in TiO_2 and Ni in NiO [19].

CORROSION

The corrosion behavior of these oxidized wires was investigated in a companion study [20]. It was shown that the corrosion resistance is a strong function of oxide thickness where samples with the thinner (<0.1μm), more pure oxides have higher corrosion resistance. It is further illustrated that the Ni-rich regions in the thicker, less pure oxides promote localized corrosion (pitting).

CONCLUSIONS

The present paper shows the phase formation and kinetics of transformations for oxidized NiTi. Electropolished wires are characterized by a thin (~0.01μm) TiO_2 layer. The thickness of the oxide layer increases with increasing oxidation time at temperature between 400˚C and 1000˚C. A Ni-rich layer is observed at the interface between NiTi and the thermal TiO_2. Above 800˚C the Ni_3Ti interfacial layer transforms into Ni_4Ti with finger-like projections (approximately 80at% Ni) and Ni islands (approximately 98at% Ni) surrounded by TiO_2. The oxidation reactions for these samples appear to proceed as follows:

$$NiTi + O_2 \rightarrow Ni_3Ti + TiO_2 \rightarrow Ni_4Ti + TiO_2 \rightarrow Ni + TiO_2$$

This oxide growth was determined to be parabolic, with a resultant activation energy of 50 kcal/mol. The parabolic nature of this oxide prevents further high-rate oxidation. The corrosion behavior of NiTi is highly dependent on the thickness and composition of these oxide layers.

REFERENCES

1. T. Duerig, A.R. Pelton, and D. Stoeckel, in *Mater Sci Eng*, A273-275, 1999, p. 149-160.
2. D. Stoeckel, in *Min Invas Ther & Allied Technol,* 9(2), 2000, p. 81-88.
3. D.E. Hodgson, M.H. Wu, and R.J. Biermann, in ASM Metals Handbook ASM, 10th ed., Vol 2, 1991, p.897-902.
4. J. Ryhanen, in *Min Invas Ther & Allied Technol*, 9(2), 2000, p.99-106.

5. C. Trepanier, R. Venugopalan, and A.R. Pelton, in Shape Memory Implants, ed. L. Yahia, 2000, p.35-45.
6. R. Venugopalan, and C. Trepanier, in *Min Invas Ther & Allied Technol,* 9(2), 2000, p. 67-74.
7. V.G. Chuprina, in *Soviet Powder Metallurgy and Metal Ceramics,* 28(4), 1989, p. 468-472.
8. J.P. Espinos, A. Fernandez, and A.R. Gonzalez-Elipe, in *Surf Sci,* 295, 1993, p. 402-410.
9. R.G. Vichev, *et al.*, in Proceeding of the Seventh European Conference on Applications of Surface and Interface Analysis, eds. I. Olefjord, L. Nyborg, and D. Briggs (Goteborg), 1997, p. 679-682.
10. C. Trepanier, *et al.*, in *J Biomed Mater Res (Appl Biomater)*, 43, 1998, p. 433-440.
11. S. Trigwell, *et al.*, in *Sufr Interface Anal*, 26, 1998, p. 483-489.
12. B.L. Pelton and J. Vitarelli, in SMST-2000: Proceedings from the International Conference on Shape Memory and Superelastic Technologies, eds. S.M Russell and A.R. Pelton, (Pacific Grove, California: International Organization on SMST-2000), p. 97-102.
13. G.S. Firstov, *et al.*, in *Biomaterials,* 22, 2002, p. 4863-4871.
14. C.L. Chu, S.K. Wu, and Y.C. Yen, in *Materials Science and Engineering*, A216, 1996, p. 193-200.
15. A.S. Khanna, High Temperature Oxidation and Corrosion, ASM International, 2002.
16. C.L. Zeng, in *Oxidation of Metals*, 58(1/2), 2002, p. 171-184.
17. D.R. Gaskell, Introduction to Metallurgical Thermodynamics, 2nd ed., 1981, p. 287.
18. V.G. Chuprina, in *Soviet Powder Metallurgy and Metal Ceramics*, 28(4), 1989, p. 310-314.
19. O. Kubaschewski and B.E. Hopkins, Oxidation of Metals and Alloys, 2nd ed., 1962.
20. C. Trepanier et al, *Corrosion Resistance of Oxidized Nitinol*, in SMST-2003: Proceedings from the International Conference on Shape Memory and Superelastic Technologies, eds. A.R. Pelton and T. Duerig, (Pacific Grove, California: SMST Society), these proceedings.